A Dual-Amplification Electrochemical Aptasensor for Profenofos Detection

Journal of The Electrochemical Society, 2020 **167** 027515

A Dual-Amplification Electrochemical Aptasensor for Profenofos Detection

Hui Zhang,[1,2,3] Jianfei Sun,[1,2,3] Shuting Cheng,[1,2,3] Huimin Liu,[1,2,3] Falan Li,[1,2,3] Yemin Guo,[1,2,3,z] and Xia Sun[1,2,3,z]

[1]*School of Agricultural Engineering and Food Science, Shandong University of Technology, Zibo 255049, People's Republic of China*
[2]*Shandong Provincial Engineering Research Center of Vegetable Safety and Quality Traceability, Zibo 255049, People's Republic of China*
[3]*Zibo City Key Laboratory of Agricultural Product Safety Traceability, Zibo 255049, People's Republic of China*

The present study reported a dual-amplification electrochemical aptasensor for sensitive detection of profenofos (PFF) in vegetables. A screen-printed carbon electrode (SPCE) modified with graphitized multi-walled carbon nanotubes ($MWCNT_{Gr}$) and Au nanoshell was used as a test platform, which ensured a rapid detection process and showed a favorable electrochemical performance. $MWCNT_{Gr}$ and Au nanoshell enhanced the electrical conductivity and the surface area, thus the detection signal was amplified. The affinity between PFF and its aptamer (Apt) was verified firstly by dot blot hybridization (DBH), and the result was exciting. Furthermore, the effects of the aptamers modified respectively with $-NH_2$ and -SH on the current signal were compared with each other by cyclic voltammetry (CV), and results showed that the aptamers modified with $-NH_2$ made the current signal change more obvious. Based on all above, a high-efficiency electrochemical aptasensor was fabricated with a wide linear range from 0.1–1 $\times$ 10^5 ng $\cdot$ ml^{-1} and a detection limit of 0.052 ng $\cdot$ ml^{-1} under the optimized conditions. This aptasensor had great specificity, stability and reproducibility. Hence, the developed aptasensor was successfully used to detect PFF in vegetables. The proposed method also has a potential for the detection of other organophosphorus pesticide (OPs).
 [DOI: 10.1149/1945-7111/ab6972]

Manuscript submitted August 16, 2019; revised manuscript received December 2, 2019. Published January 21, 2020.

Profenofos (PFF) is a kind of moderately toxic and common organophosphate insecticide widely used in agriculture today and in the future.[1,2] Its action mode is to inhibit the activity of acetylcholinesterase, while it has the effect of contact killing and gastric toxicity.[3] PFF is not only a broad spectrum organophosphorus insecticide but also acaricide. And it is easy to biodegrade, which can be used to control a variety of chewing and sucking mouth pests and mites on cotton, fruit trees, tea trees, vegetables and other crops. It is still effective against other cotton pests resistant to organophosphorus and pyrethroids.[4,5] The World Health Organization (WHO) lists PFF as a moderately hazardous (toxicity class II) pesticide.[6–8] It is necessary to detect the residue of PFF because the usage of PFF has raised a serious concern to the environment and human health.[9,10] By far, a variety of analytical methods have been developed for detection of organophosphorus pesticide (Ops) residues, such as mass spectroscopy (MS),[11] spectrophotometer,[12] gas chromatography with a nitrogen-phosphorus detector (GC-NPD),[13] enzyme-linked immunosorbent assay (ELISA)[14] or high performance liquid chromatography (HPLC).[15] Although these conventional techniques offer high selectivity and sensitivity, they are coupled with numerous shortcomings, including complex samples pretreatment, time consuming, expensiveness, sophisticated instrumentation and expert operators. Biosensors using electrodes modified chemically are alternative methods for sensitive determination of PFF, which can decrease time and cost.

Aptamers are single-stranded oligonucleotides (DNA, RNA) that can specifically bind to various target molecules.[16–18] They are selected from random oligonucleotide libraries based on systematic evolution of ligands by exponential enrichment (SELEX) technology.[19] Compared with traditional microbial culture, they have the advantages of short detection period and low detection limit, which are due to the large surface area and a mass of receptor binding sites, as well as the diversity of their spatial conformation.[20,21] The aptamers obtained by screening are easy to synthesize in large quantities *in vitro*, which have good repeatability, high stability and easy storage.[22] In addition, they have wide targets and low detection cost,[23–25] and have been widely used in cell imaging,[26] drug delivery,[27] disease treatment[28] and microbial detection[29,30] in recent years. However, aptasensors specifically for PFF are still very limited.

Dot blot hybridization (DBH) is a method of nucleic acid molecular hybridization, which has been widely used in virus detection in recent years.[31–33] DBH technology refers to the hybridization of nucleic acid probe with nucleic acid DNA of the sample to be tested on the hybridization membrane. The nucleic acid probe is equipped with appropriate markers for post-reaction detection, and combines with specific target molecules to form a hybrid body, which is then displayed by color reaction.[34] Hence, DBH can be used to detect the affinity between aptamer and PFF.

In recent years, multi-walled carbon nanotubes (MWCNTs) have attracted broad attention in scientific areas, such as chromatography, solid phase extraction techniques and particularly in electrochemical field on account of their remarkable properties.[35,36] Whereas, graphitized multi-walled carbon nanotubes ($MWCNT_{Gr}$) are more stable than MWCNTs, which have an excellent electrical conductivity that can amplify current signals and have an especial structure with interconnected network that can fix more molecules.[37–39] Furthermore, electrodes modified with $MWCNT_{Gr}$ have shown favorable electrochemical performance. Au nanoparticles have good optical performance, conductivity and biocompatibility. They are widely used in biology and medicine. Au nanoshell has high specific surface area, high loading capacity and great dispersion,[40–42] making it well applied in electrochemical analysis.

In view of above findings, we reported a method for detecting PFF residues in vegetables. A high-efficiency electrochemical aptasensor based on a screen-printed carbon electrode (SPCE) modified with $MWCNT_{Gr}$ and Au nanoshell was developed. $MWCNT_{Gr}$ motivated the electron transfer of the aptasensor owing to their good conductivity and Au nanoshell carried more aptamers because of its specific surface area, so that they amplified the detection signal effectively. Aptamers used as recognition elements were combined with these nanomaterials which had large specific surface areas to realize detection of PFF. Creatively, the affinity of the Apt to PFF was also determined by DBH. This aptasensor had a wide linear range and a lower detection limit. It could be applied for detecting PFF residues in vegetables based on its high sensitivity, high specificity and great reproducibility.

[z]E-mail: gym@sdut.edu.cn; sunxia2151@sina.com

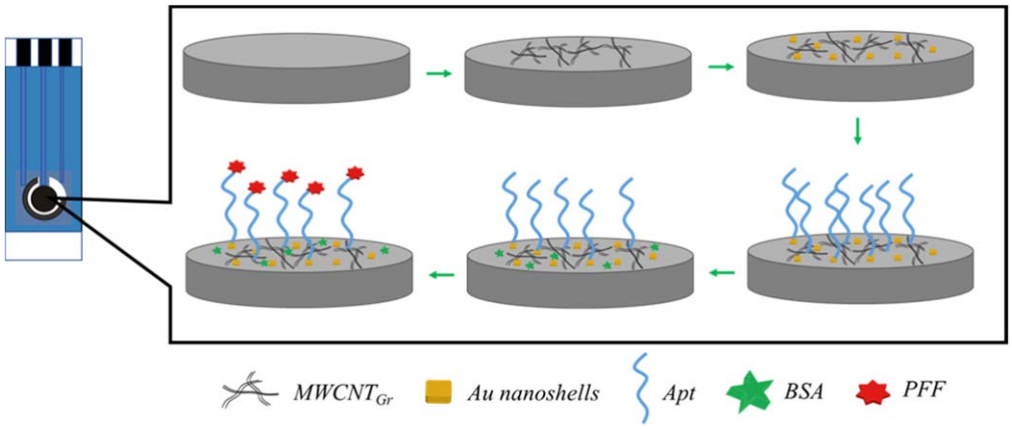

Figure 1. Procedure for the fabrication of the aptasensor.

Experimental

Reagents and apparatus.—MWCNT$_{Gr}$ was purchased from DeKe-DaoJin Co. (Beijing, China). Au nanoshell was obtained from RuiXi Biological Technology Co., Ltd. (Xi'an, China). PFF and NBT/BGIP stock solution were purchased from Sigma (USA). Bovine serum albumin (BSA) was obtained from BioDev-Tech. Co. (Beijing, China). PFF aptamer 1 (Apt 1) (5' - NH_2 - AAG CTT GCT TTA TAG CCT GCA GCG ATT CTT GAT CGG AAA AGG CTG AGA GCT ACG C − 3'), PFF aptamer 2 (Apt 2) (5' - SH - AAG CTT GCT TTA TAG CCT GCA GCG ATT CTT GAT CGG AAA AGG CTG AGA GCT ACG C − 3'), PFF aptamer 3 (Apt 3) (5' - T7 - AAG CTT GCT TTA TAG CCT GCA GCG ATT CTT GAT CGG AAA AGG CTG AGA GCT ACG C − 3') and NC membrane (0.22 μm) were purchased from Sangon Biotechnology (Shanghai, China). 5 × Transcription Buffer, DTT (1 μM), DIG and T7 RNA polymerase were purchased from Solarbio Science & Technology Co., Ltd. (Beijing). DEPC water was obtained from Thermo Fisher Scientific. Phosphate buffer solution (PBS, 0.2 M NaH_2PO_4, 0.2 M Na_2HPO_4) was be used as buffer solution to prepare 100 μM DNA stock solutions and test liquid (0.1 M KCl and 5 mM $[Fe(CN)_6]^{3-/4-}$) of this electrochemical experiment. All reagents were analytical reagent grade. All solutions were prepared with ultrapure water obtained from a LS MK2 PALL purification system (18.2 MΩ · cm).

SPCE was obtained from Zensor R&D Co. (Taiwan, TE100, China). All electrochemical measurements were carried out with a CHI660D electrochemical workstation that was purchased from CH Instruments Co. (China). The ultrasonic cleaner (SK3300H) was obtained from Kedao Ultrasonic Instrument Co., Ltd. (Shanghai, China). Scanning electron micrographs were taken by a scanning electron microscope (SEM, Quanta 250FEG) and transmission electron microscopic (TEM) images were obtained by FEI Tecnai G2F20S-TWIN 200 kV (USA).

Preparation of MWCNT$_{Gr}$ and BSA.—100 mg MWCNT$_{Gr}$ was weighed by the balance and dispersed in 50 ml ultrapure water, then ultrasonic treatment was carried out for 15 min until it became black suspension. To obtain 1% BSA solution, 4 ml ultrapure water was added to 40 mg BSA particles, stirring well and then ultrasonic treatment until dissolved completely. All the above solutions are stored in 4 °C when out of use.

Affinity determination of aptamer to PFF.—Before preparation of the aptasensor, the affinity between Apt and PFF was measured by DBH referring to the previous literature of zhang et al.[31] Using an Apt 3 as a probe template, 5 × Transcription Buffer, DTT (1 μM), DIG, T7 RNA polymerase and DEPC water were added into it. After mixing, they were put in water bath at 37 °C overnight, and 5 μl probe solution was obtained. The obtained probe solution was purified and stored at −20 °C. PFF with a series of concentration of 10 $\mu g \cdot ml^{-1}$, 1 $\mu g \cdot ml^{-1}$, 500 $ng \cdot ml^{-1}$, 100 $ng \cdot ml^{-1}$, 1 $ng \cdot ml^{-1}$ (all above were 1 μl), and 1 μl DEPC water (as reference) was orderly dripped onto the NC membrane and dried. After pre-hybridization and sealing, the detection solution and NBT/BGIP (the color rendering solution for digoxin) (the ratio was 50: 1) were added to the tube where NC film was placed, and the color rendering was observed in dark for 6 h or more.

Fabrication of the aptasensor.—Prior to modification, SPCE was prepared with a volt-amperometric cycling (−1.5 V to +1.5 V, 100 $mV \cdot s^{-1}$) during 25 cycles in 0.5 M H_2SO_4 solution, and then it was cleaned thoroughly with ultrapure water and dried under a stream of nitrogen. 6 μl MWCNT$_{Gr}$ solution pipetted onto the SPCE, then 6 μl Au nanoshell was added. The modified SPCE dried at room temperature successively. Then, 6 μl Apt solution was dropped onto the modified SPCE surface and incubated for 2 h. In this way, an aptasensor interface for PFF detection was obtained. Of course, the aptasensors were prepared respectively by Apt 1 and Apt 2 with other conditions were equal. After that, 1% BSA was added and incubated for 1 h to avoid nonspecific adsorption and block the remaining active sites. The prepared SPCE was stored at 4 °C. For determination of PFF, 6 μl PFF solution in different concentrations was incubated onto the sensing surface. Figure 1 showed the preparation processes for the fabrication of the aptasensor.

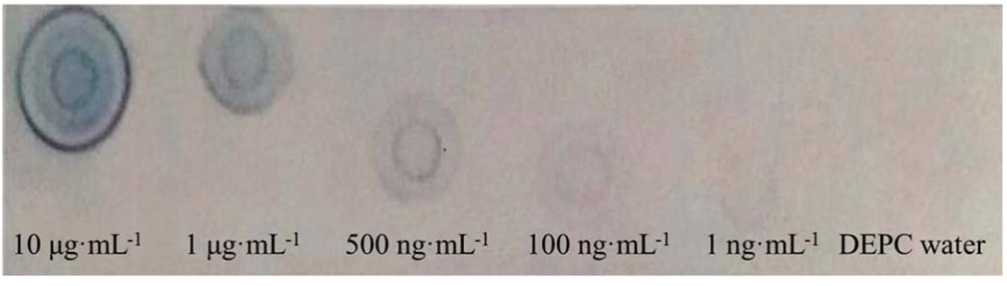

Figure 2. Affinity detection results.

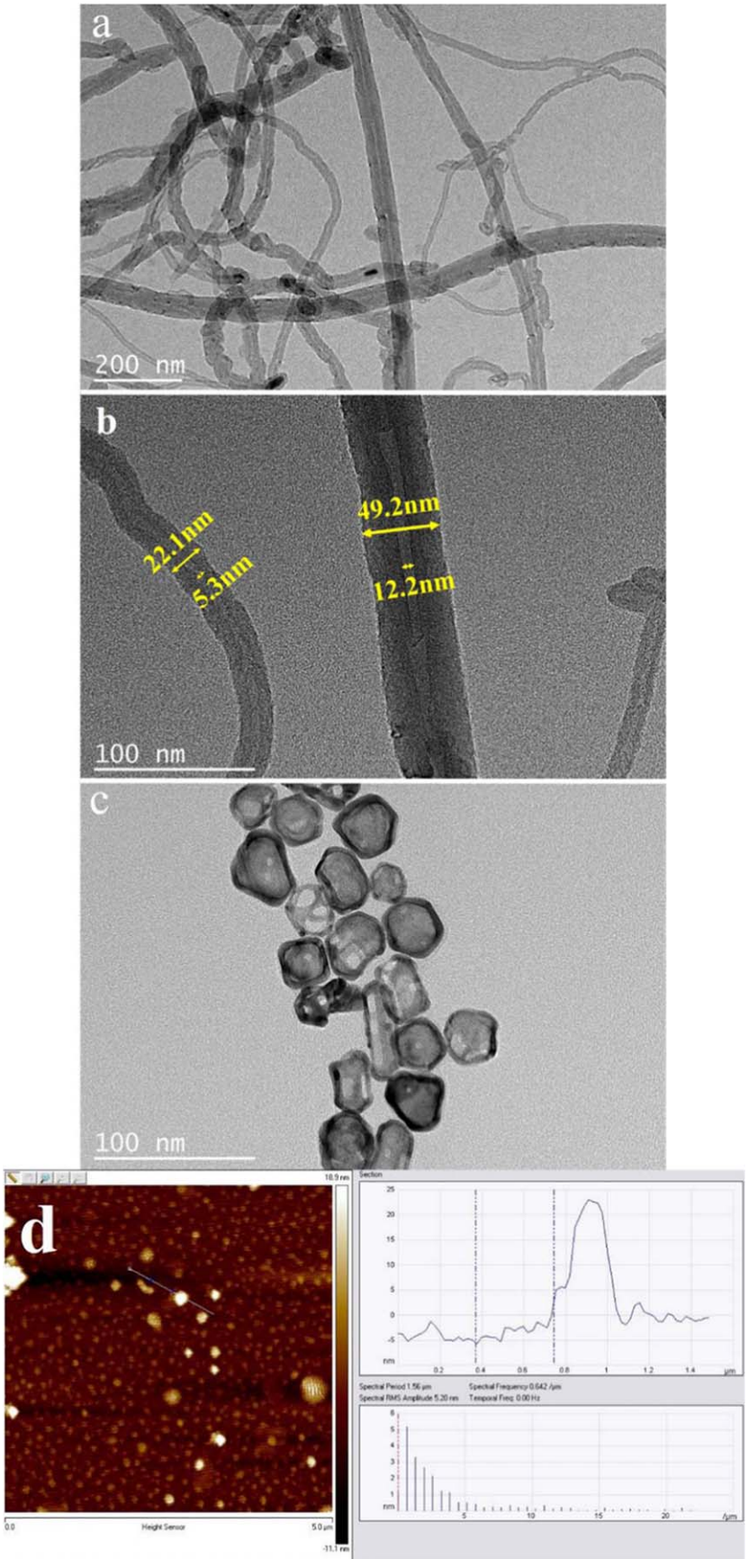

Figure 3. (a)-(b) TEM of $MWCNT_{Gr}$; (c) TEM of Au nanoshell; (d) AFM of $MWCNT_{Gr}$/Au nanoshell.

Detection of PFF with the aptasensor.—Cyclic voltammetry (CV) was performed and potential was cycled between +0.6 V and −0.2 V with scan rate of 0.05 V · s^{-1} and sample interval of 0.001 V for the PFF/ BSA/ Apt/ Au nanoshell/ $MWCNT_{Gr}$/ SPCE. Differential pulse voltammetry (DPV) was also performed and the voltage was scanned from −0.3 V to 0.6 V with amplitude of 50

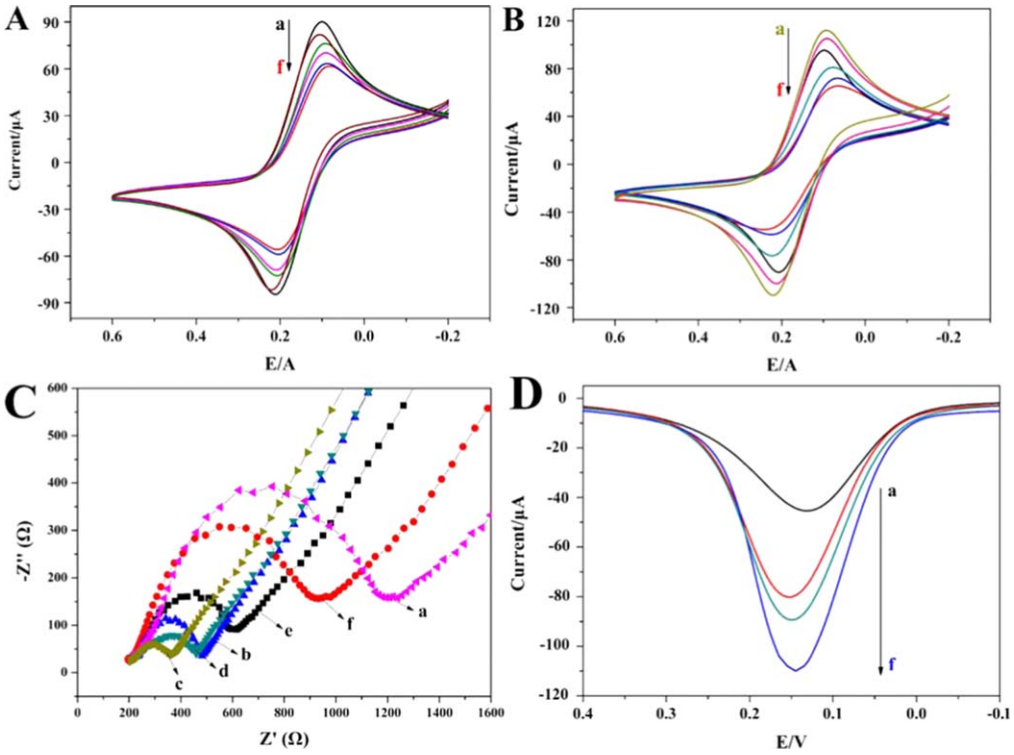

Figure 4. CV responses of different modified SPCE: (A) (a) Au nanoshell/ $MWCNT_{Gr}$/ SPCE, (b) Apt2/ Au nanoshell/ $MWCNT_{Gr}$/ SPCE, (c) $MWCNT_{Gr}$/ SPCE, (d) BSA/ Apt2/ Au nanoshell/ $MWCNT_{Gr}$/SPCE, (e) PFF/ BSA/ Apt2/ Au nanoshell/ $MWCNT_{Gr}$/ SPCE, (f) bare SPCE. (B) (a) Au nanoshell/ $MWCNT_{Gr}$/ SPCE, (b) Apt1/ Au nanoshell/ $MWCNT_{Gr}$/ SPCE, (c) $MWCNT_{Gr}$/ SPCE, (d) BSA/ Apt1/ Au nanoshell/ $MWCNT_{Gr}$/ SPCE, (e) PFF/ BSA/ Apt1/ Au nanoshell/ $MWCNT_{Gr}$/ SPCE, (f) bare SPCE. EIS of aptasensor: (C) (a) bare SPCE, (b) $MWCNT_{Gr}$/ SPCE, (c) Au nanoshell/ $MWCNT_{Gr}$/ SPCE, (d) Apt/ Au nanoshell/ $MWCNT_{Gr}$/ SPCE, (e) BSA/ Apt/ Au nanoshell/ $MWCNT_{Gr}$/ SPCE, (f) PFF/ BSA/ Apt/ Au nanoshell/ $MWCNT_{Gr}$/ SPCE. DPV responses of different modified SPCE: (D) (a) bare SPCE, (b) Au nanoshell/ SPCE, (c) $MWCNT_{Gr}$/ SPCE, (d) Au nanoshell/ $MWCNT_{Gr}$/ SPCE.

mV. All electrochemical measurements were carried out in the 0.1 M PBS containing 0.1 M KCl and 5 mM $[Fe(CN)_6]^{3-/4-}$, which served as a redox probe.

Sample preparation.—The applicability of the aptasensor was evaluated by detecting PFF levels in PFF spiked vegetables. Vegetables (cabbage, spinach and lettuce) were obtained from a local supermarket. For preparation of the juice samples, firstly vegetables were cleaned with ultrapure water and then dried in the air. Then they would be cut into pieces with 2 mm diameter. 2 g leaves were weighed and put into a small beaker. 2 ml PFF was sprayed on surface of leaves, and then they were placed at room temperature for 3 h to absorb pesticides well. After that, 1 ml acetone and 9 ml PBS (0.1 M, pH 7.5) were added, and the suspension was ultrasonic for 15 min and centrifuged at 1000 rpm for 10 min. The supernatant can be measured directly. The concentration of pesticides in the sample would be calculated according to the calibration curve.

Results and Discussion

Analytical performance of DBH.—When the target DNA (Apt 3) and PFF were molecularly hybridized, the digoxin-specific antibody added to the hybrid portion could form an enzyme-linked antibody-hapten complex with the digoxin hapten molecule, and then added the corresponding color substrate, which made the color change in the hybridization part. The color changes indicated that the Apt had successfully combined with the PFF, and the darker the color, the more PFF bound to the Apt. As shown in Fig. 2, the chromogenic degree decreased with the decreasing of PFF concentration. DEPC water was used as a negative control, so it had no color. These results demonstrated that the affinity between Apt and PFF was good.

Characterization of the nanomaterials.—The morphology and structure of different nanomaterials were showed in Fig. 3. The morphology of $MWCNT_{Gr}$ was smooth and it exhibited highly ordered graphitic structure (Fig. 3a). As seen from Fig. 3b, it can be observed that the outer diameter of $MWCNT_{Gr}$ was 20–50 nm and the inner diameter was approximately 5–12 nm. The TEM image (Fig. 3c) of Au nanoshell showed it was evenly dispersed and had a nice form with an average diameter of 33 nm. It can be seen from the Fig. 3d, the fibrous structures were $MWCNT_{Gr}$ and granular bodies were Au nanoshells. The change of height proved that this two were well combined. The height of the measured part in Fig. 3d was analyzed, and the height of the position on the surface was obviously increased, which strongly suggested the binding of $MWCNT_{Gr}$ and Au nanoshell.

Electrochemical characterization of the aptasensor.—As shown in Fig. 4, CVs had been recorded in every fixed step in the constructing of aptasensor. Due to the better redox property of $[Fe(CN)_6]^{3-/4-}$, a pair of good reversible redox peaks was observed at the bare SPCE (curve f, Figs. 4a and 4b). After modified $MWCNT_{Gr}$ onto the electrode, the redox peak increased apparently (curve c, Figs. 4a and 4b), ascribing to the unique electrical conductivity and structure of $MWCNT_{Gr}$ which could enhance the effective surface area of the SPCE to promote the electron transfer significantly. Then Au nanoshell continued to be modified onto the SPCE, and the redox peak currents further increased (curve a, Figs. 4a and 4b), which indicated that the combination of the two nanomaterials had been successfully immobilized on the SPCE surface. To further verify the good conductivity of $MWCNT_{Gr}$/ Au nanoshell, DPV was used to characterize the current increase of the SPCE modified with $MWCNT_{Gr}$, Au nanoshell and $MWCNT_{Gr}$/ Au nanoshell. As shown in Fig. 4d, Au nanoshell was separately immobilized on a bare SPCE with a current of only 80.11 μA (curve b, Fig. 4d) and $MWCNT_{Gr}$

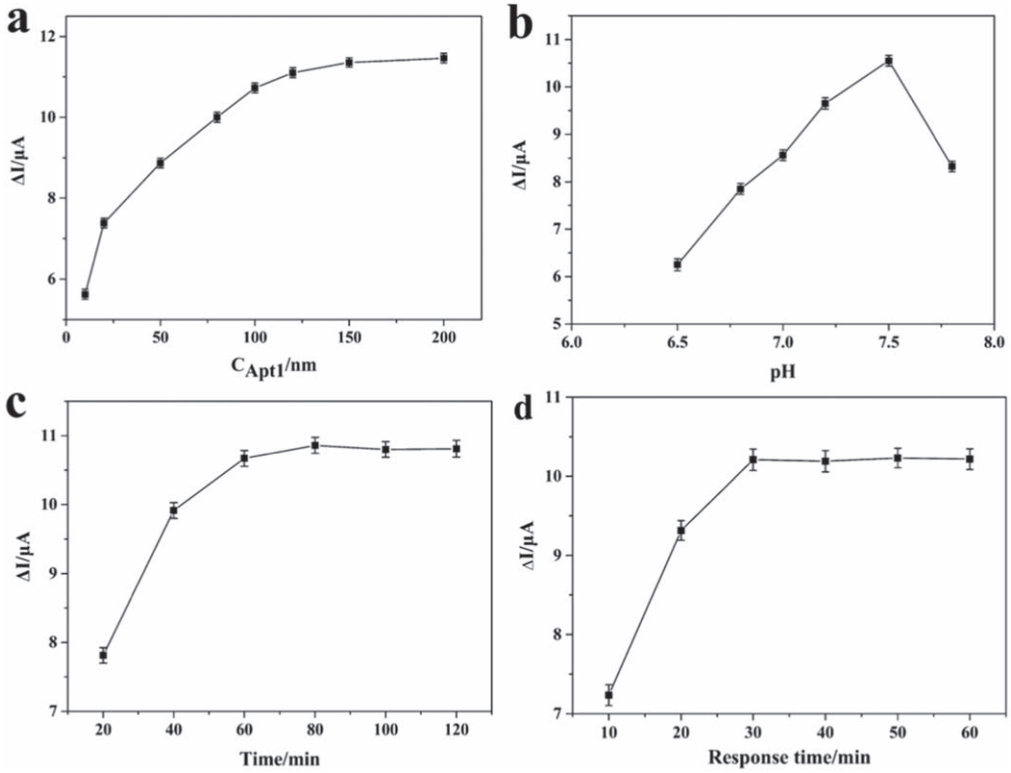

Figure 5. The influence of (a) concentration of Apt 1, (b) pH of test liquid, (c) incubation time (d) response time.

had a current of only 89.47 μA (curve c, Fig. 4d). $MWCNT_{Gr}$/ Au nanoshell were immobilized on the bare SPCE step by step with a current of 125.7 μA (curve d, Fig. 4d). The current of the $MWCNT_{Gr}$/ Au nanoshell combination was more than those of $MWCNT_{Gr}$ or Au nanoshell. Due to the oligonucleotides could generate an insulating layer to block electron transfer, the redox peak currents would be reduced (curve b, Figs. 4a and 4b) significantly with the immobilization of Apt 1 or Apt 2. Thereafter, BSA was added to block the remaining active sites, which resulted in the reduction of current (curve d, Figs. 4a and 4b). PFF and its Apt could form a complex which could hinder the electron transfer at the electrode interface, so the addition of PFF led to a further reduction of the current signal (curve e, Figs. 4a and 4b). Briefly, these results demonstrated the successful fabrication of the sensing interface.

Electrochemical impedance spectroscopy (EIS) is an effective method to further characterize the electron transfer characteristics of different modified electrodes. At the same with CV, PBS was also the test solution of EIS. The semicircle diameter of the Nyquist plot reflected the electron transfer resistance. As shown in Fig. 4c, it was observed that a clear semicircle was obtained at the bare SPCE. The semicircle diameter was shortened when the $MWCNT_{Gr}$ was dropped onto the electrode surface. The semicircle diameter was further decreased when Au nanoshell was added. Thereafter, the semicircle diameter was successive increased when the Apt, BSA and PFF were added onto the surface of SPCE respectively. Hence, the results of EIS were agreed with those of the CVs.

The current difference (ΔI) was a reference for evaluating the performance of aptasensor in this experiment, and the concentration of the target could be qualitatively analyzed on the basis of the ΔI value. We wrote the current when adding the Apt as I_0 and the current when adding PFF as I_1, so $\Delta I = I_0 - I_1$. With all other things being equal, the larger the current difference was, the more the Apt bound to PFF, so that the more accurate the detected PFF concentration would be. Therefore, it could be seen from that the ΔI in Fig. 4b was larger than that in Fig. 4a. This was the reason that nitrogen atom in $-NH_2$ was more likely to bond carbon atom in $MWCNT_{Gr}$ and SPCE to form stable C ≡ N, so that more PFF bound to the Apt and the current change was more obvious. Therefore, NH_2-modified Apt, that was Apt 1, was selected to construct the aptasensor in subsequent experiments.

Optimization of aptasensor.—To achieve a satisfactory sensing performance, the Apt 1 concentration, pH value of test liquid and incubation time were investigated and optimized. Apt concentration could affect the detection limit of the aptasensor, so different concentrations of Apt 1 were chosen to estimate the effect of the Apt concentration on the current signal which was shown in Fig. 5a. As expected, the ΔI was increased with the increase of the concentration of Apt 1, and ΔI reached the maximum value when the concentration got to 120 nM. Thus, 120 nM was chosen as the optimal concentration for constructing the aptasensor.

The effect of pH value on the aptasensor response was optimized with a different pH PBS (6.5–7.8). The ΔI increased originally with the increase of the pH value and then decreased with that, and the maximum ΔI value was obtained at pH 7.5 (Fig. 5b). Thus, pH 7.5 was the optimal pH value of the solution used for the fabrication of the aptasensor.

The incubation time of the detection system was also optimized. A series of PFF/ BSA/ Apt 1/ Au nanoshell/ $MWCNT_{Gr}$/ SPCE were incubated for 20, 40, 60, 80, 100 and 120 min. As shown in Fig. 5c, the ΔI increased with the extension of the reaction time and remained stable over 60 min. That was the consequence of the construction of Apt-PFF complex on the electrode surface reached saturation. Hence, 60 min was the optimal reaction time for subsequent experiments.

It was necessary to optimize response time which was a basic characteristic of the aptasensor. The interval of adding aptamers and PFF was 10, 20, 30, 40, 50 and 60 min, respectively. As shown in Fig. 5d, the ΔI increased with the extension of the time and remained stable over 30 min, which meant that the Apt was integrated fully with PFF. Hence, 30 min was the optimal response time for this experiment.

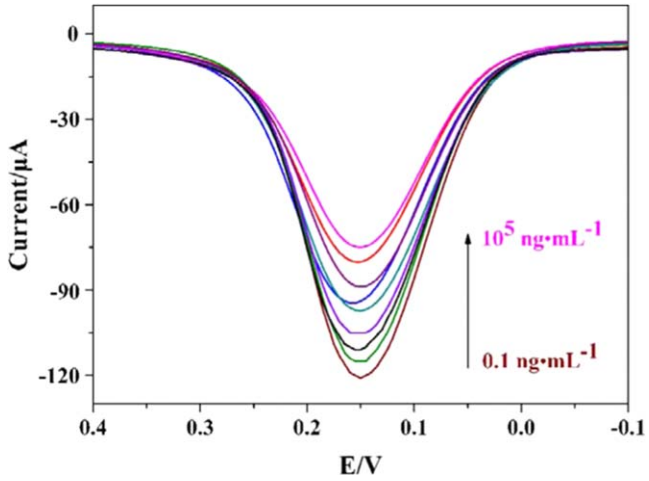

Figure 6. DPV responses to different concentrations of PFF (0.1 ng·ml^{-1}–1 × 10^5 ng·ml^{-1}).

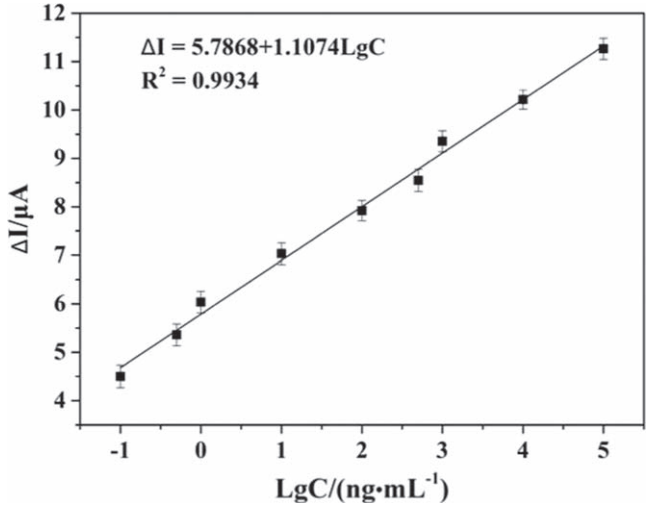

Figure 7. Calibration curve of the aptasensor.

Calibration curve of the aptasensor.—Under optimal conditions, the analytical capabilities of the developed aptasensor were investigated by DPV in different concentrations of PFF standard solutions. The combination of PFF and Apt hindered electron reaching to the electrode surface, as shown in Fig. 6, the DPV peak currents gradually decreased with increasing concentration of PFF. In the range from 0.1–1 × 10^5 ng · ml^{-1}, the linear analysis of PFF generated the following equation $\Delta I = 5.7868 + 1.1074LgC$ (Fig. 7) and the detection limit for PFF was 0.052 ng · ml^{-1} (S/N = 3), which indicated that the aptasensor had a good sensitivity. As shown in Table I, the linear range and limit of detection in this study were comparable or even better than those of other reports.

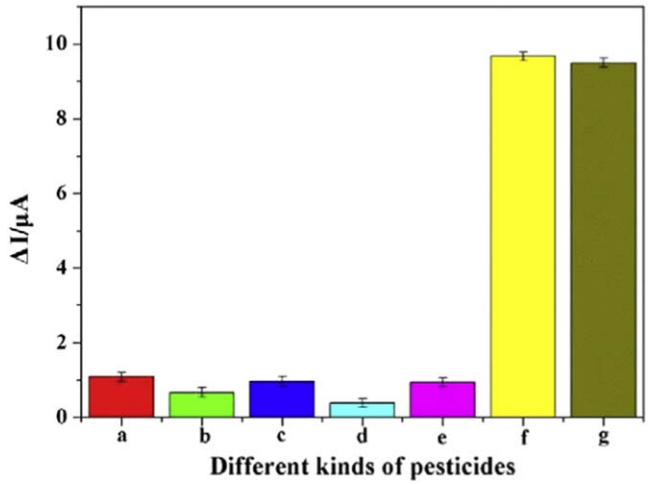

Figure 8. Selectivity assessment of the aptasensor: (a) moncrotophos; (b) omethoate; (c) phorate; (d) isocarbophos; (e) methamidophos; (f) PFF; (g) PFF, moncrotophos, omethoate, phorate, isocarbophos and methamidophos.

Specificity, stability and reproducibility of the aptasensor.—Specificity was one of the important factors which had been tested in this work to evaluate the performance of the developed aptasensor. To investigate the specificity of the aptasensor, five interfering pesticides (moncrotophos, omethoate, phorate, isocarbophos and methamidophos) were utilized to test that of the developed aptasensor (Fig. 8). No obvious response changes generated when there were only interference pesticides (Figs. 8a–8e). Compared with Fig. 8f (only the presence of PFF), Fig. 8g (PFF and five interfering pesticides) did not be different significantly. These results suggested that the proposed aptasensor had good specificity for PFF.

The reproducibility was also investigated by prepared five independent aptasensors to detect PFF in the same concentration. The relative standard deviation (RSD) was 3.52%, which showed a good reproducibility.

The prepared aptasensors were stored at 4°C for 4 weeks to detect PFF to investigate the stability of the developed aptasensor. The results revealed that the response of this aptasensor only decreased by 7.08%, which indicated a good stability in detection of PFF.

Real sample analysis.—The performance of the proposed aptasensor was further evaluated for detection of PFF by the standard addition methods in vegetables. Before the experiment, the vegetables were confirmed to contain no pesticide residue by LC. These samples were spiked at four levels (0, 0.5, 10 and 100 ng·ml^{-1}). The analytical results of three kinds of vegetables were shown in Table II. The recovery rate was in the range of 96.8%–104% with RSD between 1.44%-3.01%. These results

Table I. Comparison with other PFF detection methods.

Detection method	Linear range (nM)	Limit of detection (nM)	References
Microcantilever-array aptasensor	13.4–2.7 × 10^3	3.5	43
Aptamer-based SERS	—	14000	44
Fluorescence	5 × 10^4–5 × 10^5	11400	45
Fluorescence	300–1 × 10^4	100	46
Fluorescence	268–2.68 × 10^4	134	47
Electrochemical	1 × 10^4–2 × 10^8	2000	6
Electrochemical	3–30	2	48
Electrochemical	100–1 × 10^4	270	49
Electrochemical	0.27–2.7 × 10^5 (0.1–1 × 10^5 ng·ml^{-1})	0.14 (0.052 ng·ml^{-1})	This work

Table II. The recovery of the developed aptasensor in vegetables.

Sample	Spiked ($ng \cdot ml^{-1}$)	Total found ($ng \cdot ml^{-1}$)	Recovery (%)	RSD (%)
Spinach	0	0	—	—
	0.5	0.52	104	1.92
	10	9.87	98.7	1.44
	100	99.57	99.57	2.08
Lettuce	0	0	—	—
	0.5	0.54	108	2.93
	10	10.12	101.2	1.45
	100	100.78	100.78	1.89
Cabbage	0	0	—	—
	0.5	0.47	94	3.01
	10	9.68	96.8	2.37
	100	99.95	99.95	1.97

showed that the aptasensor had great practicability in detection of PFF in vegetables.

Conclusions

In this paper, a high-efficiency and rapid aptasensor based on MWCNTGr and Au nanoshell for determination of PFF was fabricated successfully. MWCNTGr could more tightly modify SPCE owing to their great electrical conductivity and especial structure. The combination of the MWCNTGr and Au nanoshell could effectively increase the electrical activity of the aptasensor. SPCE had advantageous in handling conveniently and portability for on-site analysis, providing a promising platform for detecting PFF sensitively in vegetables. The proposed aptasensor had high specificity, reproducibility and stability with a wide linear range from $0.1–1 \times 10^5$ $ng \cdot ml^{-1}$. The detection limit for PFF was 0.052 $ng \cdot ml^{-1}$. Therefore, the proposed aptasensor have a potential for the determination of OPs in practical applications and the method can be applied to the preparation of other sensors with good conductivity, easy modification and straight operation.

Acknowledgments

This work was supported by the National Natural Science Foundation of China (No. 31772068), Innovative project for major science and technology of Shandong Province (2018CXGC0214), Key Innovative Project for 2018 Major Agriculture Application Technology of Shandong Province.

References

1. Q. Q. Zheng, Y. Chen, K. Fan, J. Wu, and Y. B. Ying, *Anal. Chim. Acta*, **982**, 78 (2017).
2. J. W. Dong, N. Gao, Y. Peng, C. Guo, Z. Q. Lv, Y. Wang, C. H. Zhou, B. A. Ning, M. Liu, and Z. X. Gao, *Food Control*, **25**, 543 (2012).
3. S. T. Singleton et al., *Int. J. Hyg. Envir. Heal.*, **218**, 203 (2015).
4. T. Nie, R. M. Hua, F. Tang, X. W. Wu, and J. J. Tang, *Anhui Agri. Sci.*, **37**, 14323 (2009).
5. J. Luo, N. Jia, H. Y. Shi, and M. H. Wang, *Environ. Sci. Technol.*, **34**, 16 (2011).
6. M. Amatatongchai, W. Sroysee, P. Sodkrathok, N. Kesangam, C. Chairam, and P. Jarujamrus, *Anal. Chim. Acta*, **1076**, 64 (2019).
7. in *The WHO Recommended Classification of Pesticides by Hazard and Guidelines to Classification 1990–1991* (Word Health Organization) WHO/PCS/90.1 (Geneva, Switzerland) (1990).
8. A. M. Shrivastav, S. P. Usha, and B. D. Gupta, *Biosens. Bioelectron.*, **79**, 150 (2016).
9. L. M. Ravelo-Pérez, J. Hernández-Borges, and M. Á. Rodríguez-Delgado, *J. Chromatogr. A*, **1211**, 33 (2008).
10. V. P. Androutsopoulos, A. F. Hernandez, J. Liesivuori, and A. M. Tsatsakis, *Toxicology*, **307**, 89 (2013).
11. F. J. Mo, Q. Han, J. Y. Song, J. L. Wu, P. Y. Ran, and Y. Z. Fu, *J. Electrochem. Soc.*, **B679**, 165 (2018).
12. Y. Li, Q. Lu, R. Hu, Z. B. Chen, and P. Qiu, *Chinese Chem. Lett.*, **29**, 1845 (2018).
13. J. Zhang, K. Yang, and L. Chen,, *J. Electrochem. Soc.*, **B182**, 166 (2019).
14. V. Yusa, M. Millet, C. Coscolla, and M. Roca, *Anal. Chim. Acta*, **891**, 15 (2015).
15. F. Ahmadi, Y. Assadi, S. M. R. M. Hosseini, and M. Rezaee, *J. Chromatogr. A*, **1101**, 307 (2006).
16. S. Tombelli, M. Minunni, and M. Mascini, *Biosens. Bioelectron.*, **20**, 2424 (2005).
17. Z. Shekari, H. R. Zare, and A. Falahati, *J. Electrochem. Soc.*, **B739**, 164 (2017).
18. J. G. Bruno and J. L. Kiel, *Biosens. Bioelectron.*, **14**, 457 (1999).
19. C. Tuerk and L. Gold, *Science*, **249**, 505 (1990).
20. J. Yao, C. H. Liu, and M. Yang, *J. Electrochem. Soc.*, **B1161**, 166 (2019).
21. M. M. Foroughi, S. Jahani, and M. Rajaei, *J. Electrochem. Soc.*, **B1300**, 166 (2019).
22. N. Duan, S. Wu, S. Dai, H. Gu, L. Hao, H. Ye, and Z. Wang, *Analyst*, **141**, 3942 (2016).
23. A. Boussebayle, F. Groher, and B. Suess, *Methods*, **161**, 10 (2019).
24. S. Song, L. Wang, J. Li, J. L. Zhao, and C. H. Fan, *TrAC-Trend. Anal. Chem.*, **27**, 108 (2008).
25. A. B. Iliuk, L. Hu, and W. A. Tao, *Anal. Chem.*, **83**, 4440 (2011).
26. X. Chen, Y. Pan, H. Liu, X. J. Bai, N. Wang, and B. L. Zhang, *Biosens. Bioelectron.*, **79**, 353 (2016).
27. N. Hamaguchi, A. Ellington, and M. Stanton, *Anal. Biochem.*, **294**, 126 (2001).
28. O. C. Farokhzad, J. J. Cheng, B. A. Teply, I. Sherifi, S. Jon, P. W. Kantoff, J. P. Richie, and R. Langer, *P. Natl. Acad. Sci. USA*, **103**, 6315 (2006).
29. N. N. Li, X. Huang, D. P. Sun, Y. S. Zhong, and Z. G. Chen, *J. Electrochem. Soc.*, **B604**, 166 (2019).
30. Y. Li, G. J. Ran, G. Lu, X. Y. Ni, D. L. Liu, J. X. Sun, C. F. Xie, D. S. Yao, and W. B. Bai, *J. Electrochem. Soc.*, **B449**, 166 (2019).
31. C. Y. Zhang, G. F. Chen, Y. Liu, Y. Y. Wang, Z. Xu, B. Y. Zhang, and G. C. Wang, *Harmful Algae*, **35**, 9 (2014).
32. Y. C. Hsu, T. J. Yeh, and Y. C. Chang, *J. Virol. Methods*, **128**, 54 (2005).
33. V. Raja, M. Prasad, P. Bothammal, P. Saranya, K. Sumaiya, C. S. A. Mercy, and K. Natarajaseenivasan, *J. Microbiol. Meth.*, **156**, 20 (2019).
34. M. E. de Noronha Fonseca, L. H. Marcellino, and E. Gander, *J. Virol. Methods*, **5**, 203 (1996).
35. Y. Z. Keteklahijani, F. Sharif, E. P. L. Roberts, and U. Sundararaj, *J. Electrochem. Soc.*, **B1415**, 166 (2019).
36. A. Miranda, N. Barekar, and B. J. McKay, *J. Alloy. Compd.*, **774**, 820 (2019).
37. A. O. Adegbenjo, P. A. Olubambi, J. H. Potgieter, M. B. Shongwe, and M. Ramakokovhu, *Mater. Design*, **128**, 119 (2017).
38. S. F. Li, B. Sun, H. Imai, T. Mimoto, and K. Kondoh, *Compos. Part A-Appl. S.*, **48**, 57 (2013).
39. Y. Xue, S. Zheng, Z. Sun, Y. Zhang, and W. Jin, *Chemosphere*, **183**, 156 (2017).
40. M. Li, D. Wu, Y. Chen, G. Y. Shan, and Y. C. Liu, *Mater. Sci. Eng.: C*, **95**, 11 (2019).
41. Y. Gan, J. D. Sun, T. Liang, J. W. Tu, N. Hu, H. Wan, and P. Wang, *J. Electrochem. Soc.*, **B793**, 166 (2019).
42. M. P. Melancon, W. Lu, Z. Yang, R. Zhang, and Z. Cheng, *Mol. Cancer Ther.*, **7**, 1730 (2008).
43. C. Li, G. P. Zhang, S. Q. Wu, and Q. C. Zhang, *Anal. Chim. Acta*, **1020**, 116 (2018).
44. S. Pang, T. P. Labuza, and L. He, *Analyst*, **139**, 1895 (2014).
45. L. Wang, H. Ye, H. Q. Sang, and D. D. Wang, *Chinese J. Anal. Chem.*, **44**, 799 (2016).
46. T. T. Tang, J. J. Deng, M. Zhang, G. Y. Shi, and T. S. Zhou, *Talanta*, **146**, 55 (2016).
47. X. W. Dou, X. F. Chu, W. J. Kong, J. Y. Luo, and M. H. Yang, *Anal. Chim. Acta*, **891**, 291 (2015).
48. T. Liu, M. R. Xu, H. S. Yin, S. Y. Ai, X. J. Qu, and S. S. Zong, *Microchim. Acta*, **175**, 129 (2011).
49. G. Selvolini, I. Băjan, O. Hosu, C. Cristea, R. Săndulescut, and G. Marrazza, *Sensors*, **18**, 2035 (2018).